Structural Engineering and Mechanics, Vol. 12, No. 5 (2001) 475-490
DOI: http://dx.doi.org/10.12989/sem.2001.12.5.475

Remeshing techniques for *r*-adaptive and combined *h*/*r*-adaptive analysis with application to 2D/3D crack propagation*

H. Askes† and L.J. Sluys‡

Faculty of Civil Engineering and Geosciences, Koiter Institute Delft, Delft University of Technology, P.O. Box 5048, 2600 GA Delft, The Netherlands

B.B.C. de Jong‡†

TNO Building and Construction Research, P.O. Box 49, 2600 AA Delft, The Netherlands

Abstract. Remeshing strategies are formulated for *r*-adaptive and *h*/*r*-adaptive analysis of crack propagation. The relocation of the nodes, which typifies *r*-adaptivity, is a very cheap method to optimise a given discretisation since the element connectivity remains unaltered. However, the applicability is limited. To further improve the finite element mesh, a combined *h*/*r*-adaptive method is proposed in which *h*-adaptivity is applied whenever *r*-adaptivity is not capable of further improving the discretisation. Two and three-dimensional examples are presented. It is shown that the *r*-adaptive approach can optimise a discretisation at minimal computational costs. Further, the combined *h*/*r*-adaptive approach improves the performance of a fully *r*-adaptive technique while the number of *h*-remeshings is reduced compared to a fully *h*-adaptive technique.

Key words: adaptivity; remeshing; ALE; crack propagation; failure analysis; localisation.

1. Introduction

Failure analyses of real-type engineering problems often require that mechanical processes on a much smaller scale are taken into account. For instance, a proper description of cracking phenomena is needed to account for a correct simulation of structural failure. Enhanced continuum material models such as the nonlocal damage model are suited to capture the crack propagation process in a physically realistic manner (Pijaudier-Cabot and Bažant 1987, Sluys 1992). With an enhanced continuum material model the cracks are simulated as zones where strains localise, i.e., intense straining concentrates in the so-called localisation zones. Numerical solution strategies, such as the finite element method, provide the tools to carry out the simulations. However, very fine meshes are needed to capture the localised strain fields correctly. The use of overall fine meshes leads to a highly inefficient computation, since then also the zones where no cracks occur are

† Assistant Professor
‡ Associate Professor
‡† Research Engineer

*The earlier version of this paper appears in proceedings of ECCOMAS 2000, 11-14 September 2000, Barcelona, Spain.

discretised with small elements. As a consequence, the computational costs in terms of CPU time and memory requirements rise dramatically, especially in three-dimensional analysis, which precludes a straighforward application of failure analysis with continuum models to engineering practice.

In order to balance the accuracy requirements and the efficiency requirements of numerical failure analysis mesh-adaptive techniques can be applied. The aim of using mesh-adaptive techniques is to optimise the spatial discretisation such that the element size is small enough in the complete domain. The criterion with which the desired element size is computed is normally provided by the user, for instance by means of error assessment and a given error tolerance. Several adaptive techniques have been proposed in the literature, including *h*-adaptivity, *p*-adaptivity and *r*-adaptivity (Zienkiewicz and Zhu 1991, Huerta *et al.* 1999). *h*-adaptive schemes change the mesh connectivity constantly through the addition or deletion of elements. The enrichment of the polynomial interpolation space in certain regions, which characterises *p*-adaptivity, requires special interface constructions between elements with different interpolation polynomials. The relocation of nodes with invariant element connectivity as occurs in *r*-adaptive schemes prohibits the addition or deletion of degrees of freedom regardless of an initially too coarse or too dense mesh. Whereas *h*-adaptive schemes and *p*-adaptive schemes are suitable for achieving a *prescribed accuracy* upon repeated refinement, *r*-adaptive schemes can make an *optimal use* of a given mesh topology, so that reasonable solutions can be obtained at minimal computational costs. Indeed, it has been shown that the computational overhead of *r*-adaptive schemes can be made negligible. More specifically, the difference in computer costs of analyses with and without *r*-adaptivity can be made as low as $\mathcal{O}(N)$ with N the number of elements (Rodríguez-Ferran *et al.* 1998, Askes and Sluys 2000, Askes 2000). In contrast, the continuous construction of a completely new mesh as it is done in *h*-adaptivity can be a time-consuming task, especially in a three-dimensional analysis.

However, the applicability of *r*-adaptivity is limited since the number of degrees of freedom and the element connectivity cannot be changed. For a more flexible formulation, *r*-adaptivity and *h*-adaptivity can be combined. Indeed, the advantages of *h*-adaptivity and *r*-adaptivity are complementary. Whereas *r*-adaptivity is a cheap adaptive technique which can be used to optimise a given finite element configuration, *h*-adaptivity can be applied to construct a new mesh whenever *r*-adaptivity is not capable of further improving the mesh. Therefore, a combined *h*/*r*-adaptive approach is more flexible than a fully *r*-adaptive approach, so that the limitations of *r*-adaptivity can be overcome. On the other hand, a combined *h*/*r*-adaptive scheme can be more efficient than a fully *h*-adaptive scheme, since at certain stages *r*-adaptive remeshing can be used instead of the more expensive *h*-adaptive remeshing.

In this study we formulate *r*-adaptive and *h*/*r*-adaptive strategies for the analysis of crack propagation. A heuristic error indicator is derived from an analysis of dispersive waves (Huerta and Pijaudier-Cabot 1994, Sluys *et al.* 1995, Askes 2000). With this error indicator remeshing strategies are elaborated which allow for mesh refinement in the zones of interest, i.e. cracked zones and zones where cracking is about to occur. Two and three-dimensional examples show the performances and the limitations of each of the approaches.

2. Nonlocal damage theory

An isotropic damage theory is used in which the stresses $\underline{\sigma}$ are related to the strains $\underline{\varepsilon}$ as

$$\underline{\sigma} = (1 - \omega)\underline{D}\,\underline{\varepsilon} \tag{1}$$

in which ω is the scalar damage and $\underline{D}$ contains the elastic stiffness moduli. Damage growth is determined via an equivalent strain ε_{eq} which is defined as (Peerlings *et al.* 1998)

$$\varepsilon_{eq} = \frac{(k_{ct} - 1)I_1}{2k_{ct}(1 - 2\nu)} + \frac{1}{2k_{ct}}\sqrt{\frac{(k_{ct} - 1)^2 I_1^2}{(1 - 2\nu)^2} + \frac{2k_{ct}J_2}{(1 + \nu)^2}} \tag{2}$$

where k_{ct} denotes the ratio of compressive strength over tensile strength (taken here as $k_{ct} = 10$) while the strain invariants I_1 and J_2 are defined as

$$I_1 = \varepsilon_1 + \varepsilon_2 + \varepsilon_3 \tag{3}$$

$$J_2 = (\varepsilon_1 - \varepsilon_2)^2 + (\varepsilon_2 - \varepsilon_3)^2 + (\varepsilon_3 - \varepsilon_1)^2 \tag{4}$$

with ε_1, ε_2 and ε_3 the principal strains. A damage loading function is defined as $f = \varepsilon_{eq} - \kappa$ where the history parameter $\kappa = \max(\varepsilon_{eq}, \kappa_i)$ and the damage threshold κ_i is a material parameter. If $f = 0$ and $\dot{f} = 0$ then damage grows according to

$$\omega = 1 - \frac{1}{1 + b(\varepsilon_{eq} - \kappa_i)} \tag{5}$$

with b a parameter that sets the softening behaviour of the material.

The above model lacks a parameter that sets the *width* of the zone in which damage grows. Mathematically, this becomes manifest in the ill-posedness of the mechanical equations in the softening regime. Numerically, the finite element solutions strongly depend on the applied element size. To overcome these deficiencies, a nonlocal formalism is taken in that the equivalent strain is averaged over a representative volume as (Pijaudier-Cabot and Bažant 1987)

$$\bar{\varepsilon}_{eq(x)} = \frac{\int_V \alpha_{(s)}\varepsilon_{eq(x+s)}dV}{\int_V \alpha_{(s)}dV} \tag{6}$$

In Eq. (6), the weighting function $\alpha_{(s)}$ sets the representative volume. It is normally taken as a decaying non-negative function. Here, the error function is taken as $\alpha_{(s)} = \exp(-|s|/2l_c^2)$ where l_c is a length scale parameter that sets the size of the averaging volume in Eq. (6). The *nonlocal* equivalent strain $\bar{\varepsilon}_{eq}$ replaces the *local* equivalent strain ε_{eq} in the damage loading function and the damage evolution function (5). As a consequence, the length scale l_c sets the size of the damaging zone, so that mathematically well-posed differential equations result and mesh-objective results can be obtained (Pijaudier-Cabot and Bažant 1987, Bodé 1994).

3. Determination of the desired element sizes

While a nonlocal framework in the constitutive relations can guarantee mesh-objective solutions in the whole loading process, mesh-adaptivity is needed to make failure analyses available for engineering practice. Without adaptive techniques, computational analysis either becomes very inefficient (when a fine mesh is used in the whole domain) or inaccurate (when a coarse mesh is used in the whole domain). Adaptive procedures can generally be considered to consist of two

stages. Firstly, the error of the numerical solution must be assessed, and secondly this information on the error must be translated into an improved mesh which is expected to meet the error tolerances. This section deals with error assessment, while the adaption of the finite element mesh is discussed in the next section.

Following the terminology of Huerta *et al.* (1999), we distinguish between *error estimators* on one hand and *error indicators* on the other. The former provide an *estimation* of the true error, which can be derived from mathematical considerations, and are mostly expensive in terms of computer time. The latter do not approximate the magnitude of the true error but only give an *indication* where the error is large and where it is small. Normally, they can be determined directly from the state variables, which make them cheap to compute (Huerta *et al.* 1999). In either case, the error quantity must be translated into a pointwise defined desired element size to serve as an input for the remeshing algorithm.

Below, we use a dispersion analysis to derive ad-hoc formulae to compute a desired element size. Dispersion properties of a material model set the ability to transform a wave of a certain wave length into waves with different wave lengths. It has been shown that dispersive properties are crucial in the regularisation of a material model (Sluys 1992, Huerta and Pijaudier-Cabot 1994). Furthermore, when dispersion properties of the continuum model are compared to that of the discretised model, the influence of the discretisation can be assessed (Huerta and Pijaudier-Cabot 1994, Sluys *et al.* 1995). This latter approach will be followed here to relate the dispersion properties of the material to a desired size of the applied finite elements.

In an infinitely long one-dimensional medium, a harmonic perturbation of the displacement field yields the phase velocity c as a function of the (assumedly uniform) strain state ε_0 (see Sluys 1992, Huerta and Pijaudier-Cabot 1994, Bodé 1994 for details of the derivation). For the nonlocal damage model applied in this study, the phase velocity is expressed as

$$\frac{c^2}{c_e^2} = (1-\omega_0) - \varepsilon_0 \frac{\partial \omega}{\partial \bar{\varepsilon}_{eq}} \exp\left(-\frac{k^2 l_c^2}{2}\right) \tag{7}$$

where $c_e = \sqrt{E/\rho}$ is the one-dimensional tensile wave velocity, E is Young's modulus, ρ is the mass density, ω_0 is the uniform damage state that corresponds to ε_0 and k is the wave number for which the phase velocity c is computed. In dynamic analyses, the wave velocity c must be real (Sluys 1992, Huerta and Pijaudier-Cabot 1994, Sluys *et al.* 1995, Peerlings *et al.* 1996). Equivalently, in static analyses $c = 0$ (Bodé 1994, Sluys *et al.* 1995). As such, a *critical wave number* k_{crit} can be derived above which the right hand side in Eq. (7) is positive. Next, a *critical wave length* λ_{crit} can be derived by using $\lambda = 2\pi/k$ (Sluys 1992, Huerta and Pijaudier-Cabot 1994, Peerlings *et al.* 1996) as

$$\lambda_{\text{crit}} = \frac{\sqrt{2}\pi l_c}{\sqrt{\ln b + \ln \varepsilon_0 - \ln(1 + b(\varepsilon_0 - \kappa_i))}} \tag{8}$$

where Eq. (5) has been substituted. This critical wave length is the maximum wave length that can still propagate through the damaged zone (Sluys 1992, Sluys *et al.* 1995). It sets the width of the zone over which damage can grow (Sluys 1992, Sluys *et al.* 1995, Peerlings *et al.* 1996). Thus, Eq. (8) relates the width of the localisation zone to the strain level. Note that the critical wave length λ_{crit} is directly proportional to the internal length scale l_c.

Eq. (8) gives the critical wave length for a *continuous* medium, i.e. prior to finite element discretisation. In a similar manner, an expression for the critical wave length in a *discretised* medium can be found (Sluys *et al.* 1995). This latter expression relates the critical wave length not only to the strain level, but also to the applied element size. An upper bound on the deviation between approximate (numerical) critical wave length and the exact (continous) critical wave length then leads to an upper bound for the element size. For instance, for a gradient-dependent plastic material it has been derived that 12 linear finite elements are needed to capture the localisation zone if a 10% mismatch between discrete critical wave length and continuous critical wave length is accepted (Sluys *et al.* 1995). As such, dispersion analysis can be used to derive an error measure which in the terminology of Huerta *et al.* (1999) is denoted an *error indicator.* An advantage is that the error indicator only depends on the state variables and the discretisation measures, which are readily available. Thus, the error indicator is cheap to compute. On the other hand, when a different material model or different damage loading function is used, the behaviour of the error indicator changes.

Numerical experimentation confirms the above reasoning. One-dimensional simulations of strain-softening problems have shown that a certain number of elements over the localisation zone is needed to obtain a reasonable approximation of the localisation zone. For the nonlocal damage model employed in this study, 10-15 elements over the localisation zone seems to give a satisfactory description of the damaging zone (Pijaudier-Cabot and Bažant 1987, Bodé 1994, Askes and Sluys 2000).

Combining the analytical considerations of dispersion analysis with the numerical experimentation, we use the expression of the critical wave length Eq. (8) to determine an element size that is deemed suitable to capture the damage and strain fields adequately. This element size will be denoted the *desired element size* in the sequel. Simple formulae are postulated that relate the desired element size to the strain level, with the requirement that the desired element size remains well below the critical wave length, so that it is guaranteed that a large enough number of elements is used inside the localisation zone. For the elements in which damage takes place an expression that meets this requirement reads

$$\text{desired element size} = h_1 - (h_1 - h_2)\omega \tag{9}$$

where h_1 is the desired element size for $\omega = 0$ or $\bar{\varepsilon}_{eq} = \kappa_i$, and h_2 is the desired element size for $\omega = 1$. By setting values for h_1 and h_2, implicitly an error tolerance is provided. In Fig. 1 the critical wave length and the desired element size (both normalised with respect to the internal length scale l_c) are plotted as a function of the strain level, for a range of values for h_1 and h_2. In this figure, $\kappa_i = 3.5 \times 10^{-4}$ and $b = 20000$. For the chosen range of h_1 and h_2 the desired element sizes are smaller than the critical wave length.

While the above arguments give a desired element size for inelastic zones, a sufficiently fine mesh is equally important in the elastic zones. Too large elements in the elastic regions can significantly delay or disturb the crack initiation and crack propagation processes (Askes *et al.* 1999, Askes and Sluys 1999, Askes and Sluys 2000). Therefore, it should be ensured that element sizes are small enough in regions where cracking is about to occur. To this end, a desired size is also defined for elements that are still undamaged. Obviously, the desired element size should be a continuous function of the strain level. Similar to Eq. (9) we define for the elastic regime

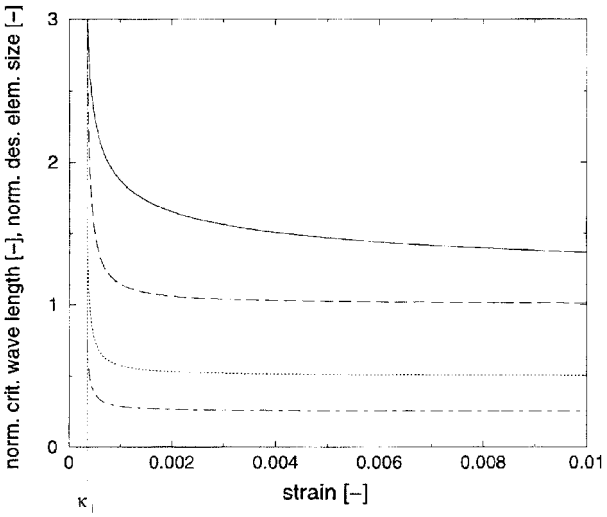

Fig. 1 Normalised critical wave length (solid) and normalised desired element size for $h_2/l_c = 1$ (dashed), $h_2/l_c = 0.5$ (dotted) and $h_2/l_c = 0.25$ (dot-dashed), $h_1/h_2 = 3$ for all cases

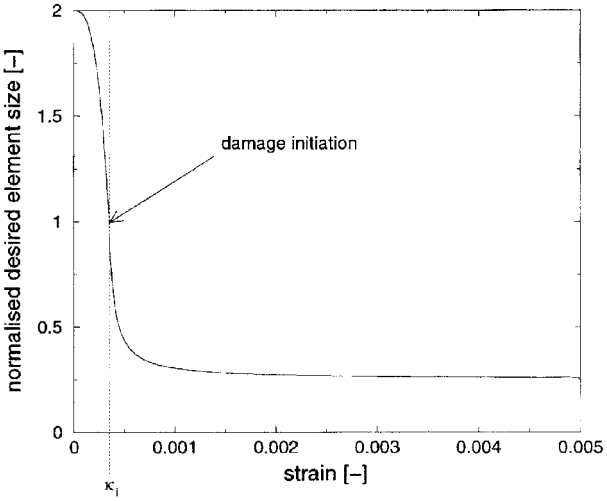

Fig. 2 Desired element size normalised with respect to internal length scale versus strain level–elastic and inelastic regime

$$\text{desired element size} = h_0 - (h_0 - h_1)\left(\frac{\bar{\varepsilon}_{eq}}{\kappa_i}\right)^n \tag{10}$$

in which h_0 is the desired size for elements where no strains are present. The ratio $\bar{\varepsilon}_{eq}/\kappa_i$ denotes how close an element is to damage initiation (Askes *et al.* 1999, Askes and Sluys 2000), while the power n allows for a progressive decrease of the desired element size in the elastic regime (Askes and Sluys 2000). Note that for damage initiation, i.e. $\bar{\varepsilon}_{eq} = \kappa_i$, Eqs. (9) and (10) yield the same desired element size. In Fig. 2 the desired element size as a function of the strain level has been plotted for $h_0/l_c = 2$, $h_1/l_c = 1$, $h_2/l_c = 0.25$ and $n = 3$. Around the stage of damage initiation the

desired element size changes most rapidly, while for very small strains and very large strains the desired element size does not change much. For very large strains, this means that little *additional* refinement is performed once a damage zone has been formed.

4. Remeshing strategy

The desired element sizes, determined in the previous section, are used as input in the remeshing stage. Different remeshing strategies are formulated for *r*-adaptive remeshing and for combined *h*/*r*-adaptive remeshing. For the *r*-adaptive framework an Arbitrary Lagrangian-Eulerian (Hughes *et al*. 1981, Donéa 1983, Huerta and Casadei 1994) context is taken.

4.1 r-adaptive remeshing

In an *r*-adaptive context, nodes can be relocated so that element sizes can be adjusted in the entire domain. However, no degrees of freedom can be added. The optimal mesh is therefore obtained by equidistributing the error quantity, that is, by requiring that the product of error and element size yields the same value for each element. Since for linear elements the error is inversely proportional to the desired element size h_{des} (Díez and Huerta 1999), the equidistribution condition is written as (Bodé 1994, Pijaudier-Cabot *et al*. 1995, Askes and Sluys 2000, Askes 2000)

$$\frac{\partial}{\partial \chi}\left(\frac{1}{h_{\text{des}}} \frac{\partial x}{\partial \chi} \right) = 0 \tag{11}$$

where x are the spatial coordinates of the nodes, i.e., the unknowns that have to be solved for, and χ is a reference coordinate system associated with the mesh, i.e., each node has a unique and invariant reference coordinate χ (Hughes *et al*. 1981, Donéa 1983, Huerta and Casadei 1994).

Eq. (11) can be repeated for each spatial coordinate. Thus, a system of differential equations is found that is nonlinear since $h_{\text{des}} = h_{\text{des}}(x)$. Boundary conditions are imposed such that boundary nodes can only move *along* the boundary (Huerta and Casadei 1994). Directly applying a Galerkin variational principle to Eq. (11) yields a system of algebraic equations as

$$\underline{A}\,\underline{x} = \underline{b} \tag{12}$$

where $\underline{x}$ is the discretised unknowns, i.e. the spatial coordinates of each node, $\underline{A}$ is given by

$$\underline{A} = \int_V \sum_{\xi = x_1, x_2, x_3} \frac{\partial H^T}{\partial \xi} \frac{1}{h_{\text{des}}} \frac{\partial H}{\partial \xi} dV \tag{13}$$

and $\underline{b}$ contains the known components of $\underline{A}\,\underline{x}$ that follow from the boundary conditions. The matrix $\underline{H}$ contains the shape functions in the χ-coordinate system, that is, $\underline{H}$ should be invariant and does not change after remeshing is carried out (Askes and Sluys 2000). Eq. (12) will be referred to as the *elliptic equidistribution equation*, since it ensues from the elliptic Eq. (11). Since Eq. (11) is nonlinear, Eq. (12) must be solved iteratively. With multiple matrix inversions this form a major drawback, therefore it has been proposed to modify the right-hand-side of Eq. (11) as (Bodé 1994,

Bodé *et al.* 1995, Askes and Sluys 2000, Askes 2000)

$$\frac{\partial}{\partial \chi}\left(\frac{1}{h_{\text{des}}}\frac{\partial x}{\partial \chi}\right) = \frac{\partial x}{\partial \tau} \tag{14}$$

where a pseudo-time τ has been introduced that has no physical meaning but is only used for computational convenience. Eq. (14) can be solved by means of relaxation. Discretisation yields (Askes and Sluys 2000, Askes 2000)

$$-\underline{A}\underline{x}+\underline{b} = \underline{Q}\frac{\partial \underline{x}}{\partial \tau} \tag{15}$$

where $\underline{A}$ and $\underline{b}$ are the same as in Eq. (12) and with

$$\underline{Q} = \int_V \underline{H}^T\underline{H}dV \tag{16}$$

Eq. (15) can be solved by means of a Forward Euler scheme, e.g. When matrix $\underline{Q}$ is lumped, no matrix inversion has to be carried out, so that the solving of Eq. (15) is very efficient compared to the solving of Eq. (12). Eq. (15) is denoted the *parabolic equidistribution equation*, as it follows from the parabolic Eq. (14). It has been argued that taking the pseudo-time step $\Delta\tau < h_2^2$ leads to stable solutions with the Forward Euler scheme (Askes and Sluys 2000).

After the new nodal coordinates have been found, the stresses, strains and internal variables are transported to the new mesh using a Godunov algorithm (Huerta *et al.* 1995, Rodrígue-Ferran *et al.* 1998, Askes *et al.* 1998, Askes *et al*. 1999). For elements with one integration point, the value of a state variable component after remeshing η^{new} is related to the value before remeshing η^{old} via

$$\eta^{\text{new}} = \eta^{\text{old}}+\frac{1}{2V^{\text{el}}}\sum_{s=1}^{N_s} F_s\left(\eta^{\text{old}} - \eta^{\text{old}}_{\text{adj}}\right)(1-\text{sign}(F_s)) \tag{17}$$

where V^{el} is the element volume, N_s is the number of sides of the element, $\eta^{\text{old}}_{\text{adj}}$ is the value of η^{old} in the element adjacent to side s, and the flux F_s through side s is given by

$$F_s = \int_s -\underline{n}^T\Delta\underline{x}ds \tag{18}$$

with $\underline{n}$ the normal to side s and $\Delta\underline{x}$ the mesh incremental displacements, i.e. the mesh displacements that follow from Eq. (12) or Eq. (15). Extenstion towards elements with multiple integration points is straightforward (Huerta *et al.* 1995, Rodríguez-Ferran *et al.* 1998, Askes *et al.* 1998, Askes *et al.* 1999). Note that the computer costs involved with Eq. (17) are $\mathcal{O}(N)$, which also holds for *r*-adaptive remeshing with the parabolic equidistribution Eq. (15) (Askes and Sluys 2000).

4.2 h/r-adaptive remeshing

One of the disadvantages of *r*-adaptive remeshing is that the number of degrees of freedom remains fixed to the initial number. When this initial number is too low to capture all the characteristics of the simulation properly, *r*-adaptivity will not provide accurate solutions. Similarly, the element connectivity is invariant in *r*-adaptivity. If remeshing leads to badly shaped elements, then the accuracy may drop. As an enhancement to the fully *r*-adaptive approach, a combination of

h-adaptivity and *r*-adaptivity is proposed. Here, *r*-adaptivity is used as the default remeshing tool, while *h*-adaptivity is applied whenever *r*-adaptivity is not suitable of further improvement of the mesh.

To assess the remeshing capacities of *r*-adaptivity objectively, the concepts of Refinement Ratio and Aspect Ratio are introduced as

$$RR = \frac{\text{current element size}}{\text{desired element size}} \tag{19}$$

and

$$AR = \frac{\text{longest side of triangle}}{\text{shortest height of triangle}} \tag{20}$$

respectively. Obviously, values of *RR* and *AR* close to one are optimal, while larger values indicate a need for mesh adaption. The following algorithm is used in this study:

1. An *r*-adaptive step is performed.
2. If the resulting mesh leads to too high values for *AR* or *RR*, then the *r*-adapted mesh is discarded and *h*-adaptivity is carried out.

Performing an *r*-adaptive step while it is unknown whether this will lead to an acceptable discretisation seems a waste of computer time. However, since the computer costs associated with *r*-adaptivity are as low as $\mathcal{O}(N)$ this is acceptable.

The remeshing strategy for combined *h*/*r*-adaptivity now splits into two strategies, namely one for *h*-adaptivity and one for *r*-adaptivity. For *h*-adaptivity the computed desired element sizes are used directly as input for the mesh generator. Thus, the quality of the mesh generator determines the effectivity of *h*-adaptivity. After a new mesh has been constructed, the state variables are projected from the old mesh onto the new mesh by means of the interpolation algorithm proposed by Ortiz and Quigley (1991). For each integration point in the new mesh the corresponding element in the old mesh must be found. Sophisticated search algorithms are needed to limit the computer time that is necessary for this projection of the state variables, while a computational effort of $\mathcal{O}(N)$ seems theoretically impossible.

For the *r*-adaptive steps in the combined approach the algorithm of Section 4.1 is taken as the starting point. However, Eqs. (11) and (14) cannot be applied straightforwardly. The reason is that the reference coordinates χ are fixed on the mesh and should be invariant during the analysis. However, when an *h*-adaptive step is performed, the reference coordinates lose sense. It would be preferable to express Eqs. (11) and (14) in terms of the *current* configuration, rather than terms of the *reference* or *initial* configuration. Therefore, the derivatives with respect to χ are rewritten into derivatives with respect to the *current* spatial coordinates of the nodes using the chain rule (Askes and Rodríguez-Ferran 2001, Askes 2000). For instance, Eq. (11) then becomes

$$\frac{\partial}{\partial x_{\text{cur}}}\left(\frac{1}{h_{\text{des}}}\frac{\partial x}{\partial x_{\text{cur}}}\frac{\partial x_{\text{cur}}}{\partial \chi}\right)\frac{\partial x_{\text{cur}}}{\partial \chi} = 0 \tag{21}$$

The ratio $\partial x_{\text{cur}}/\partial\chi$ is non-zero and it is proportional to the current element size (Askes and Rodríguez-Ferran 2001). Therefore, Eq. (21) can be elaborated as

$$\frac{\partial}{\partial x_{\text{cur}}}\left(RR\frac{\partial x}{\partial x_{\text{cur}}}\right) = 0 \tag{22}$$

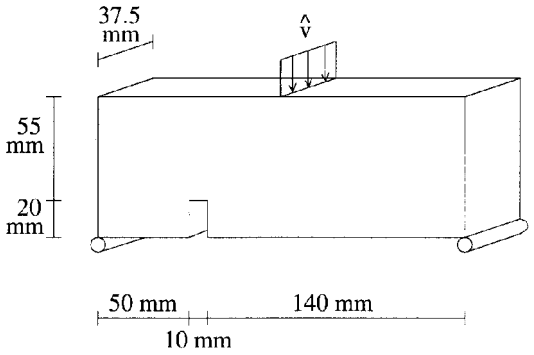

Fig. 3 Beam with eccentric notch–problem statement

Eq. (22) only contains quantities associated with the *current* configuration. Thus, generality is preserved. The parabolic equidistribution Eq. (14) can be transformed in a similar manner.

5. Examples

Two examples are presented here. The first concerns with the remeshing capacities of *r*-adaptivity, while the second example deals with *h*/*r*-adaptivity.

5.1 Dynamically loaded beam with eccentric notch

A three-dimensional dynamically loaded beam is studied. An eccentric notch is present, which drives the formation of a cracked zone that starts at the notch tip and propagates towards the top of the specimen. The geometry and loading conditions are given in Fig. 3. The imposed velocity increases linearly from $\hat{v} = 0$ mm/s at time $t = 0$ s to $\hat{v} = 2$ mm/s at time $t = 2 \cdot 10^{-4}$ s, after which it remains constant. The material parameters are taken as $E = 31000$ N/mm^2, $\nu = 0.2$, $\rho = 2.4 \cdot 10^{-9}$ Ns/mm^4, $l_c = 2$ mm, $\kappa_i = 3.5 \cdot 10^{-4}$ and $b = 20000$. Two meshes have been used, one consisting of 9393 linear tetrahedrons and one consisting of 1503 linear tetrahedrons. Both meshes are non-uniform in the sense that the mesh density is larger in the area around the notch. The finer mesh is only used in a non-adaptive analysis. With the coarser mesh a non-adaptive analysis as well as *r*-adaptive analyses have been carried out. For the *r*-adaptive analyses the values h_0/h_1 and h_0/h_2 are taken as 2 and 5, respectively[1]. Equidistribution is carried out with the elliptic equation as well as with the parabolic equation. For the parabolic equation the pseudo-time step $\Delta\tau = 0.05$.

Fig. 4 shows the damage contours for the four analyses at time $t = 10^{-3}$ s. The fine non-adaptive mesh gives a damage pattern where the crack propagates from the notch upwards with a specific inclination angle. When the coarse non-adaptive mesh is considered, it can be seen that the inclination angle does not correspond to that of the fine non-adaptive mesh. Also, the damage

[1]Eq. (11) can be multiplied with h_0. Then, the same spatial coordinates are found for the nodes, while the equidistributed error quantity is scaled with a factor h_0. In other words, *r*-adaptive remeshing is a relative process. Therefore, instead of prescribing values for h_0, h_1 and h_2, it is equality possible to prescribe the ratios h_1/h_0 and h_2/h_0.

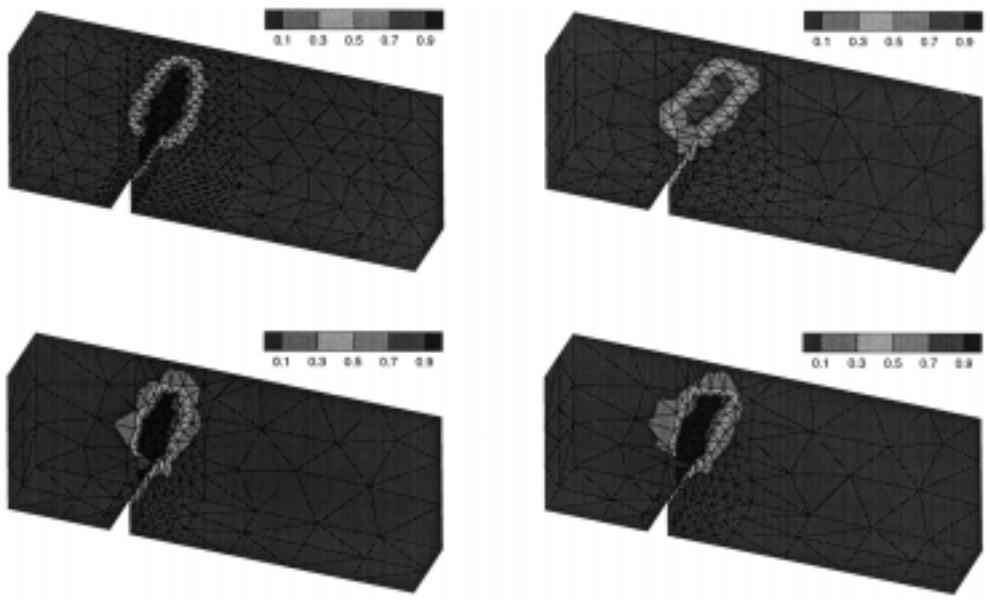

Fig. 4 Beam with eccentric notch–damage contours for fine non-adaptive mesh (upper left), coarse non-adaptive mesh (upper right), *r*-adaptive mesh with elliptic equidistribution (lower left) and *r*-adaptive mesh with parabolic equidistribution (lower right)

values inside the cracked zone are not predicted correctly. On the other hand, when the same coarse mesh is used as the initial mesh in an *r*-adaptive context, much better results are obtained. For the adaptive analyses, both the inclination angle and the maximum damage values inside the cracked zone are in good agreement with the fine non-adaptive mesh. Thus, by adjusting the nodal coordinates, the accuracy of a fine mesh can be attained by a much coarser mesh.

A next observation is that the performance of the two equidistribution equations is similar. Although minor differences are present, both capture the inclination angle and the peak damage values properly.

However, as can be seen from the adaptive meshes in Fig. 4, not much further improvement of the discretisation is possible. The number of available elements precludes that newly appearing cracks could be described adequately. Moreover, the aspect ratios of the elements above the cracked zone have become very large, which can be a source of inaccuracy. When further mesh refinement

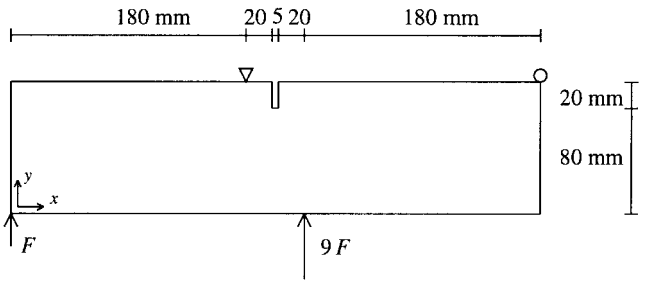

Fig. 5 Single-edge-notched beam–problem statement

is desired, a new mesh has to be constructed.

5.2 Single-edge-notched beam

In the second example we study a single-edge-notched beam. The beam is subjected to a static four-point loading, which results in the formation of a curved crack that starts at the notch tip. Furthermore, a secondary, bending crack may appear opposite of the centremost support. The material parameters are taken as $E = 30000$ N/mm^2, $\nu = 0.2$, $l_c = 1$ mm, $\kappa_i = 1.2 \cdot 10^{-4}$ and $b = 20000$. The load platens are modelled with a 10 times higher Young's modulus. An indirect displacement control procedure is used to apply the load (de Borst 1987), whereby the crack mouth sliding displacement (CMSD) is used as the control parameter. The CMSD is defined as the difference in vertical displacement between the two top nodes at either side of the notch. Two non-adaptive meshes have been used, one consisting of 11419 elements and one of 1761 elements. The finer mesh is selected such that it has an element size of 1.5 mm in the central region. Furthermore, a

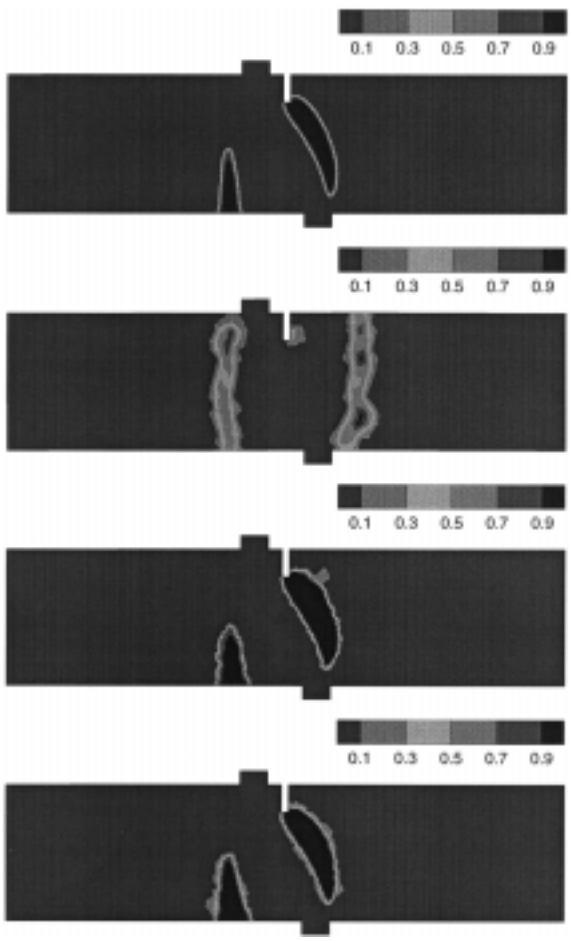

Fig. 6 Single-edge-notched beam–damage contours for CMSD = 0.04 mm, fine non-adaptive mesh, coarse non-adaptive mesh, *h*-adaptive mesh and *h*/*r*-adaptive mesh (top to bottom)

combined *h*/*r*-adaptive analysis has also been carried out whereby the coarse non-adaptive mesh is taken as the initial mesh. The desired element size is computed with $h_0 = 7$ mm, $h_1 = 3$ mm and $h_2 = 1$ mm. An *h*-adaptive step is carried out whenever the refinement ratio of an element exceeds the value 1.5 or when the aspect ratio exceeds the value 4. As a comparison, also an *h*-adaptive analysis is carried out where remeshing is performed when $RR > 1.5$.

Fig. 6 shows the damage contours for the four analyses for CMSD = 0.04 mm (note that meshes are not shown here). A first observation is the large differences in response between the two non-adaptive meshes. Whereas the finer mesh gives a crack pattern that corresponds well to known results from literature (Peerlings *et al.* 1998), the coarser mesh predicts a completely different failure mode. Due to the coarse discretisation at the notch tip, the stress singularity cannot be captured properly and the dominant, curved crack cannot develop. Alternatively, two bending cracks appear at either side of the beam. Obviously, this is due to the incapabilities of the mesh to describe the correct failure pattern.

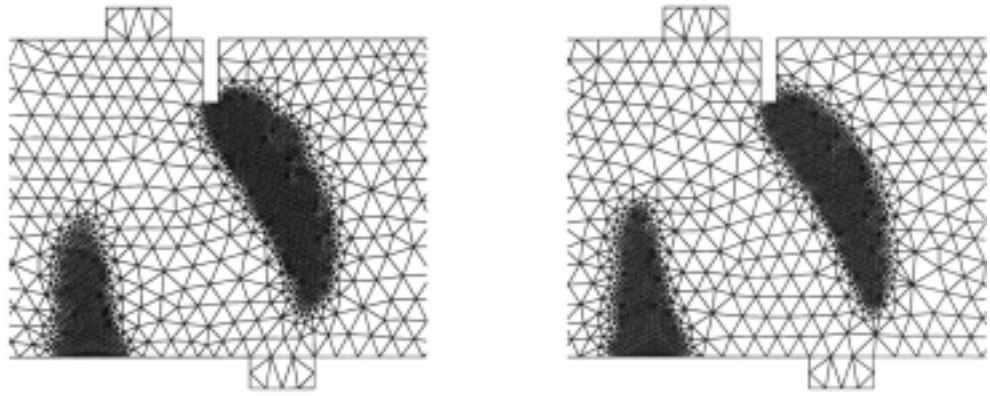

Fig. 7 Single-edge-notched beam–final meshes, zoom of central mesh section for *h*-adaptive analysis (left) and *h*/*r*-adaptive analysis (right)

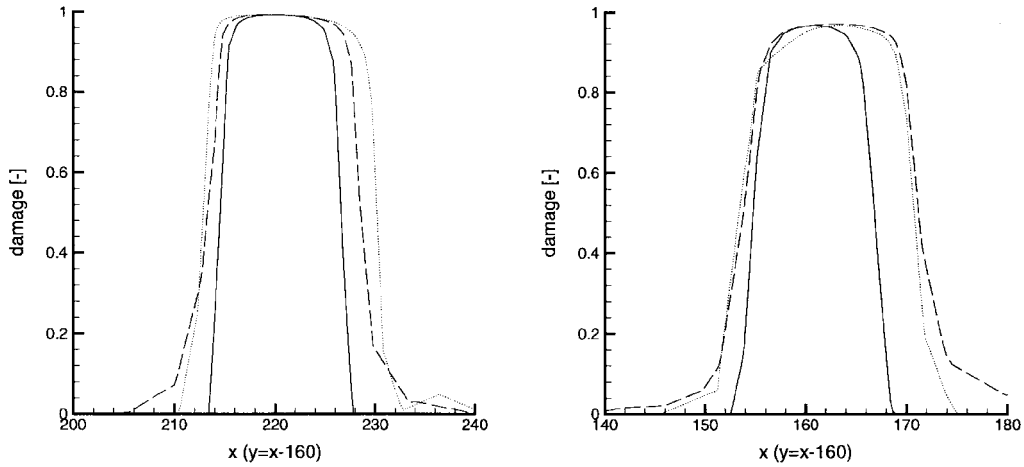

Fig. 8 Single-edge-notched beam–damage profiles for CMSD = 0.04 mm along the lines $y = x–160$ (left) and $y = 20$ (right), fine Lagrangian analysis (solid), *h*-adaptive analysis (dotted) and *h*/*r*-adaptive analysis (dashed)

The situation is different for the two adaptive analyses. In Fig. 7 a zoom of the central mesh section is given for the final configuration. For these two cases, the crack pattern is predicted correctly, while also the damage values inside the cracked zone correspond well with those of the fine non-adaptive mesh. Fig. 8 offers a closer inspection of the crack patterns, namely the damage profiles along the lines $y = x-160$ and $y = 20$ for the fine non-adaptive mesh and the two adaptive meshes. Although both adaptive meshes overestimate the crack width somewhat, the basic trends are captured reasonably well.

Fig. 9 shows the number of elements during the analysis for the two adaptive computations. Horizontal line segments denote that no remeshing is performed (*h*-adaptive test) or that *r*-adaptive

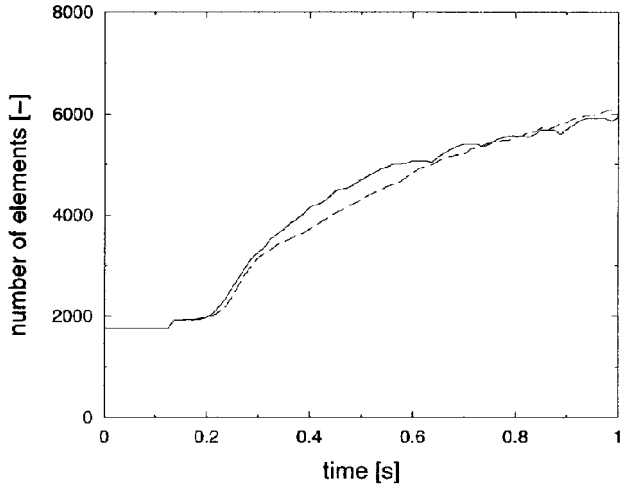

Fig. 9 Single-edge-notched beam–number of elements during the analysis, *h*-adaptive mesh (dashed) and *h*/*r*-adaptive mesh (solid)

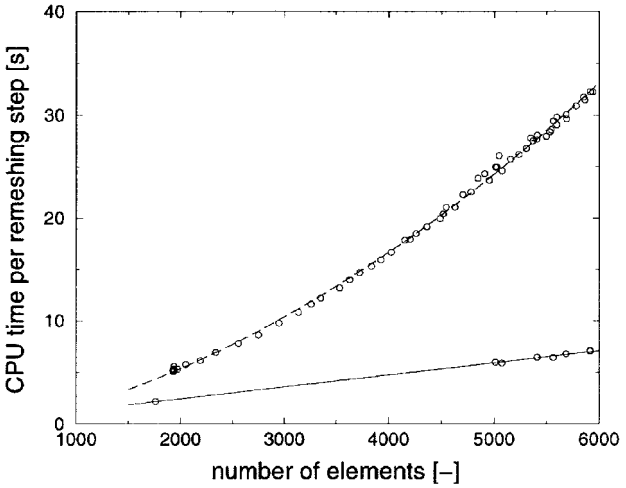

Fig. 10 Single-edge-notched beam–CPU time per remeshing step versus number of elements in the combined *h*/*r*-adaptive test, *h*-adaptive steps (dashed) and *r*-adaptive steps (solid)

remeshing is carried out (*h*/*r*-adaptive test). The number of *h*-adaptive remeshings is 69 in the *h*-adaptive test and 58 in the *h*/*r*-adaptive test. From Fig. 9 it can be seen that in the middle stages of the computation the number of *h*-remeshings is approximately the same for both tests. This corresponds to the stage where the cracks propagate relatively fast. Then, *r*-adaptivity is less suited for remeshing purposes. In the final stages of the computation, when little additional cracking takes place, *r*-adaptivity is better suited to optimise the mesh. In Fig. 10 the CPU time per remeshing step is plotted as a function of the number of elements for *r*-adaptive steps and *h*-adaptive steps in the combined *h*/*r*-adaptive analysis. A least squares approximation has been used to fit a parabolic curve through the data. It can be seen that for the *h*-adaptive steps the CPU time per step increases more than linearly with the number of elements. On the other hand, for the *r*-adaptive steps the CPU time is virtually a linear function of the number of elements. Fig. 10 confirms the $\mathcal{O}(N)$ computer costs of *r*-adaptivity as compared to the higher costs involved with *h*-adaptivity.

6. Conclusions

Remeshing strategies are formulated and tested for the analysis of crack propagation. The nonlocal damage model is used to simulate the softening material behaviour. Based on the dispersive properties of the material, heuristic formulae are proposed to compute the desired element size as a function of the strain level. The desired element size is used as input for *r*-adaptive remeshing and for a combination of *r*-adaptivity with *h*-adaptivity. *r*-adaptivity is very cheap, while *h*-adaptivity is more flexible. Examples are presented which show that *r*-adaptivity is able to optimise a given mesh topology. The accuracy of a fine non-adaptive mesh can be approximated by a simple adjustment of the nodal coordinates. However, the applicability of *r*-adaptivity is limited. The combined *h*/*r*-adaptive approach is more flexible than a fully *r*-adaptive approach in the sense that the number of elements can be changed during the analysis. On the other hand, the combined *h*/*r*-adaptive approach reduces the number of *h*-remeshings needed, so that computer costs are limited.

Acknowledgements

This research is supported by the Technology Foundation STW, applied science division of NWO and the technology programme of the Ministry of Economic Affairs, The Netherlands.

References

Askes, H. (2000), “Advanced spatial discretisation strategies for localised failure–mesh adaptivity and meshless methods”, Dissertation, Delft University of Technology.

Askes, H., Bodé, L., and Sluys, L.J. (1998), “ALE analyses of localization in wave propagation problems”, *Mechanics of Cohesive-Frictional Materials*, **3**, 105-125.

Askes, H., and Rodríguez-Ferran, A. (2001), “A combined *rh*-adaptive scheme based on domain subdivision–formulation and linear examples”, *Int. J. Numer. Meth. in Eng.*, **51**, 253-273.

Askes, H., Rodríguez-Ferran, A., and Huerta, A. (1999), “Adaptive analysis of yield line patterns in plates with

the arbitrary Lagrangian-Eulerian method", *Comput. and Struct.*, **70**, 257-271.
Askes, H., and Sluys, L.J. (1999), "Adaptive ALE analyses of crack propagation with a continuum material model", *Europ. Conf. on Computational Mechanics−Solids, Structures and Coupled Problems in Engineering*, Wunderlich W., ed., TU München.
Askes, H., and Sluys, L.J. (2000), "Remeshing strategies for adaptive ALE analysis of strain localisation", *European J. Mechanics A/Solids*, **19**, 447-467.
Bodé, L. (1994), "Stratégies numériques pour la prévision de la ruine des structures du génie civil", Dissertation, E.N.S. de Cachan/CNRS/Université Paris 6.
Bodé, L., Pijaudier-Cabot, G., and Huerta, A. (1995), "ALE finite element analysis of strain localisation−consistent computational strategy and remeshing issues", *Computational Plasticity IV*, Owen D.R.J., Oñate, E., Hinton, E., eds., Pineridge Press, Swansea, UK. 587-598.
de Borst, R. (1987), "Computation of post-bifurcation and post-failure behavior of strain-softening solids", *Comput. and Struct.*, **25**, 211-224.
Díez, P., and Huerta, A. (1999), "A unified approach to remeshing strategies for finite element h-adaptivity", *Comput. Meth. in Appl. Mech. and Eng.*, **176**, 215-229.
Donéa, J. (1983), "Arbitrary Lagrangian-Eulerian finite element methods", *Comput. for Transient Analysis*, Belytschko, T., Hughes, T.J.R., eds., Elsevier, chapter 10, 474-516.
Huerta, A., and Casadei, F. (1994), "New ALE applications in non-linear fast-transient solid dynamics", *Eng. Comput.*, **11**, 317-345.
Huerta, A., Casadei, F., and Donéa, J. (1995), "ALE stress update in transient plasticity problems", Computational Plasticity IV, Owen, D.R.J., Oñate, E., Hinton, E., eds., Pineridge Press, Swansea, UK, 1865-1876.
Huerta, A., and Pijaudier-Cabot, G. (1994), "Discretization influence on the regularization by two localization limiters", *J. Eng. Mech.*, ASCE, **120**, 1198-1218.
Huerta, A., Rodríguez-Ferran, A., Díez, P., and Sarrate, J. (1999), "Adaptive finite element strategies based on error assessment", *Int. J. Numer. Meth. in Eng.*, **46**, 1803-1818.
Hughes, T.J.R., Liu, W.K., and Zimmermann, T.K. (1981), "Lagrangian-Eulerian finite element formulation for incompressible viscous flows", *Comput. Meth. Appl. Mech. and Eng.*, **29**, 329-349.
Ortiz, M., and Quigley, J.J. (1991), "Adaptive mesh refinement in strain localization problems", *Comput. Meth. in Appl. Mech. and Eng.*, **90**, 781-804.
Peerlings, R.H.J., de Borst, R., Brekelmans, W.A.M., de Vree, J.H.P., and Spee, I. (1996), "Some observations on localisation in non-local and gradient damage models", *Europ. J. of Mech., A/Solids*, **15**, 937-953.
Peerlings, R.H.J., de Borst, R., Brekelmans, W.A.M., and Geers, M.G.D. (1998), "Gradient-enhanced damage modelling of concrete fracture", *Mechanics of Cohesive-Frictional Materials*, **3**, 323-342.
Pijaudier-Cabot G., and Bažant, Z.P. (1987), "Nonlocal damage theory", ASCE *J. Eng. Mech.*, **113**, 1512-1533.
Pijaudier-Cabot, G., Bodé, L., and Huerta, A. (1995), "Arbitrary Lagrangian-Eulerian finite element analysis of strain localization in transient problems", *Int. J. Numer. Meth. in Eng.*, **38**, 4171-4191.
Rodríguez-Ferran, A., Casadei, F., and Huerta, A. (1998), "ALE stress update for transient and quasistatic processes", *Int. J. Numer. Meth. in Eng.*, **43**, 241-262.
Sluys, J.J. (1992), "Wave propagation, localisation and dispersion in softening solids", Dissertation, Delft University of Technology.
Sluys, L.J., Cauvern, M., and de Borst, R. (1995), "Discretization influence in strain-softening problems", *Eng. Comput.*, **12**, 209-228.
Zienkiewicz, O.C., and Zhu, J.Z. (1991), "Adaptivity and mesh generation", *Int. J. Numer. Meth. in Eng.*, **32**, 783-810.